Two-Dimensional Electronic Spectroscopy for Three-Level Atoms with Electromagnetically Induced Transparency

Jing-Yi-Ran Jin, ¹ Hao-Yue Zhang, ¹ Yi-Xuan Yao, ¹ and Qing Ai^{1,*}

¹Department of Physics, Applied Optics Beijing Area Major Laboratory, Beijing Normal University, Beijing 100875, China

(Dated: January 17, 2024)

Two-dimensional electronic spectroscopy (2DES) has high spectral resolution and is a useful tool for studying atom dynamics. In this paper, we apply the electromagnetically induced transparency (EIT) technique to 2DES in a three-level atom, and find out that the number of peaks (troughs) will become more due to the introduction of EIT. Also, the height of the peaks (the depth of troughs) will change from constant to a damped oscillation. These findings may help us obtain more information about the dynamics of excited states.

I. INTRODUCTION

Electromagnetically induced transparency (EIT) is an atomic coherence effect produced by a multi-level atomic system in the presence of an external light field [1]. It can be specifically described as when the control and probe fields are incident on the system with the two-photon resonance condition, the nonlinear effects of the medium are enhanced and thus the absorption and dispersion properties are significantly altered due to the destructive interference effect between the excitation paths. Because of its unique optical properties, EIT has a wide range of applications in cold atoms [2–4], solid materials [5–9], nitrogen-vacancy color centers in diamond [10–13], quantum information processing [14–21], metamaterials [22–26], and non-reciprocal optics [27], since it was first experimentally observed by Harris' group in 1991 [28].

Two-dimensional electronic spectroscopy (2DES) is a third-order nonlinear spectral measurement technique [29], which can reflect the absorption characteristics. Three ultrafast optical coherent pulses interact with matter sequentially, and the collected optical signals containing the evolution information are transformed by double Fourier transforms to obtain 2DES. Compared with widely-used narrowband-excitation and widespectrum detection methods, 2DES can have high spectral resolution and time resolution in the case of wideband excitation. Thus, it can capture the quantum coherent phenomenon in the early stage of optical excitation [30, 31]. It can measure the homogeneous and inhomogeneous broadening of the sample [32], and also identify the coupling between different transitions by cross peaks [33]. Therefore, it plays a vital role in the investigation of the quantum dot [34, 35], twodimensional materials [36, 37], perovskite [38–40], and energy-transfer mechanism of photosynthesis [41–47]. In this paper, we apply the EIT to the 2DES for a three-level configuration and find out that the spectral resolution can be improved, which is more helpful for exploring excited-state dynamics.

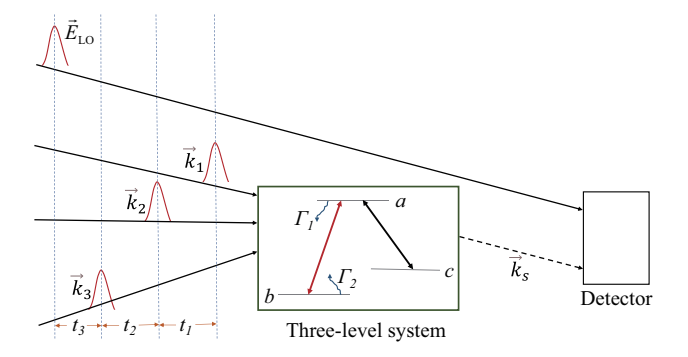


FIG. 1. Schematic diagram for 2DES of a three-level atom, where energy levels b and c are respectively the ground and metastable states, and energy level a is the excited state. Γ_1 and Γ_2 represent the relaxation rates between the energy levels a and b.

This paper is organized as follows. In Sec. II, we derive the response functions of rephasing and non-rephasing signals under the established model by using Feynman diagrams. In Sec. III, we show 2DES of rephasing, non-rephasing and absorptive signals in the presence and absence of a control field. We compare 2DES before and after introducing EIT and analyze the underlying physical mechanism of this phenomenon. In Sec. IV, we summarize our main findings.

II. MODEL

For the three-level atom as shown in the Fig. 1, four short pulses in the time domain compose a detection pulse sequence, and the time intervals between them are respectively t_1 , t_2 and t_3 . The first three detection pulses interact with the sample and resonantly probe the transition between the ground state b and the excited state a. According to the condition of the phase matching, the wave vector \vec{k}_s of the generated third-order polarization signal is the sum of the wave vectors of all the input fields, and thus a fourth pulse in this direction will be emitted. Since the signal is weak,

^{*} aiqing@bnu.edu.cn

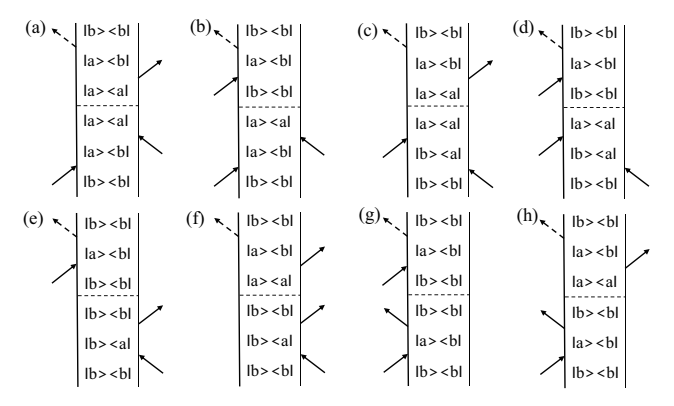


FIG. 2. Feynman diagrams for the three-level system, with R_1 for (a) and (b), R_2 for (c) and (d), R_3 for (e) and (f), and R_4 for (g) and (h).

a pulse $\vec{E}_{\rm LO}$ in the same direction as \vec{k}_s is used as the local oscillating light for heterodyne measurement. In addition, a narrow-band control light is applied in resonance with the transition between the excited state a and the metastable state c. In this way, we construct a simple Λ -type electromagnetically induced transparent model for the 2DES.

In experiments, there are three types of observable signals, i.e., the absorptive signal

$$S_{\rm ab}^{(3)}(\omega_3, t_2, \omega_1) = \operatorname{Re} \sum_{i=1}^4 R_i(\omega_3, t_2, \omega_1),$$
 (1)

the rephasing signal

$$S_{\rm rp}^{(3)}(\omega_3, t_2, \omega_1) = \text{Re}[R_2(\omega_3, t_2, \omega_1) + R_3(\omega_3, t_2, \omega_1)](2)$$

the non-rephasing signal

$$S_{\rm nr}^{(3)}(\omega_3, t_2, \omega_1) = \text{Re}[R_1(\omega_3, t_2, \omega_1) + R_4(\omega_3, t_2, \omega_1)]$$
(3)

where the different Liouville paths R_{α} 's ($\alpha = 1, 2, 3, 4$) are schematically illustrated in Fig. 2.

During the population time t_2 , R_1 and R_2 represent the initial evolution of the electron in the excited states, while R_3 and R_4 represent the initial evolution of the electron in the ground state. On the other hand, R_2 and R_3 indicate that the signal responds in the direction with the wave vector $\vec{k}_s = -\vec{k}_1 + \vec{k}_2 + \vec{k}_3$, while R_1 and R_4 indicate that the signal responds in the direction with the wave vector $\vec{k}_s = \vec{k}_1 - \vec{k}_2 + \vec{k}_3$.

For the Λ -type three-level atom as considered in Fig. 1, the Hamiltonian can be expressed as

$$H = H_0 + H_{\text{int}}, \tag{4}$$

$$H_0 = \sum_{j=a,b,c} \hbar \omega_j |j\rangle\langle j|, \tag{5}$$

$$H_{\rm int} = -\frac{\hbar}{2} \Omega e^{-i\nu_c t} |a\rangle\langle c| + \text{h.c.},$$
 (6)

where $\hbar\omega_j$ is the energy of the state $|j\rangle$ with \hbar being the reduced Planck constant, $\Omega = \mu_{ac}\varepsilon_c/\hbar$ is the Rabi frequency, ν_c and ε_c are respectively the frequency and amplitude of the control field, $\mu_{ac}=\langle a|\mu|c\rangle$ is the transition dipole moment.

In the presence of control light, the reduced density matrix of the system is governed by the quantum master equation [48]

$$\dot{\rho} = -\frac{i}{\hbar} [H, \rho] - \Gamma_1 \mathcal{L}(|b\rangle\langle a|)\rho - \Gamma_2 \mathcal{L}(|a\rangle\langle b|)\rho - \sum_{\alpha = a,b,c} \gamma_{\alpha}^{(0)} \mathcal{L}(|\alpha\rangle\langle \alpha|)\rho,$$
 (7)

where the Lindblad operator

$$\mathcal{L}(A)\rho = \frac{1}{2} \{A^{\dagger}A, \rho\} - A^{\dagger}\rho A, \tag{8}$$

 $\{A, \rho\} = A\rho + \rho A$ is the anti-commutator. Γ_1 and Γ_2 are respectively the downhill and uphill relaxation rates between the energy levels a and b. $\gamma_{\alpha}^{(0)}$ ($\alpha = a, b, c$) is the pure-dephasing noise of the state $|\alpha\rangle$.

By transforming to the interaction picture, after some algebra, we can obtain a set of differential equations for the matrix elements of ρ as

$$\dot{\rho}_{bb} = \Gamma_1 \rho_{aa} - \Gamma_2 \rho_{bb}, \tag{9}$$

$$\dot{\rho}_{ba} = -\frac{i}{2}\Omega\rho_{bc} - \gamma_1\rho_{ba},\tag{10}$$

$$\dot{\rho}_{bc} = -\frac{i}{2}\Omega\rho_{ba} - \gamma_2\rho_{bc},\tag{11}$$

$$\dot{\rho}_{ab} = \frac{i}{2} \Omega \rho_{cb} - \gamma_1 \rho_{ab}, \tag{12}$$

$$\dot{\rho}_{aa} = \frac{i}{2}\Omega(\rho_{ca} - \rho_{ac}) - \Gamma_1 \rho_{aa} + \Gamma_2 \rho_{bb}, \qquad (13)$$

$$\dot{\rho}_{ac} = \frac{i}{2}\Omega(\rho_{cc} - \rho_{aa}) - \gamma_3 \rho_{ac}, \tag{14}$$

$$\dot{\rho}_{cb} = \frac{i}{2} \Omega \rho_{ab} - \gamma_2 \rho_{cb}, \tag{15}$$

$$\dot{\rho}_{ca} = \frac{i}{2}\Omega(\rho_{aa} - \rho_{cc}) - \gamma_3 \rho_{ca}, \tag{16}$$

$$\dot{\rho}_{cc} = \frac{i}{2} \Omega(\rho_{ac} - \rho_{ca}), \tag{17}$$

where for simplicity we introduce

$$\gamma_1 = \frac{1}{2} (\Gamma_1 + \gamma_a^{(0)} + \Gamma_2 + \gamma_b^{(0)}),$$
 (18)

$$\gamma_2 = \frac{1}{2} (\Gamma_2 + \gamma_b^{(0)} + \gamma_c^{(0)}), \tag{19}$$

$$\gamma_3 = \frac{1}{2} (\Gamma_1 + \gamma_a^{(0)} + \gamma_c^{(0)}). \tag{20}$$

The relevant Green's functions are explicitly obtained as

$$\mathcal{G}_{ba,ba}(\omega_1) = \frac{4(\omega_1 - i\gamma_2 - \omega_{ab})}{4(\omega_1 - i\gamma_1 - \omega_{ab})(\omega_1 - i\gamma_2 - \omega_{ab}) - \Omega^2},$$

$$\mathcal{G}_{ab,ab}(\omega_3) = \frac{4(\omega_3 + i\gamma_2 - \omega_{ab})}{4(\omega_3 + i\gamma_1 - \omega_{ab})(\omega_3 + i\gamma_2 - \omega_{ab}) - \Omega^2},$$
(21)

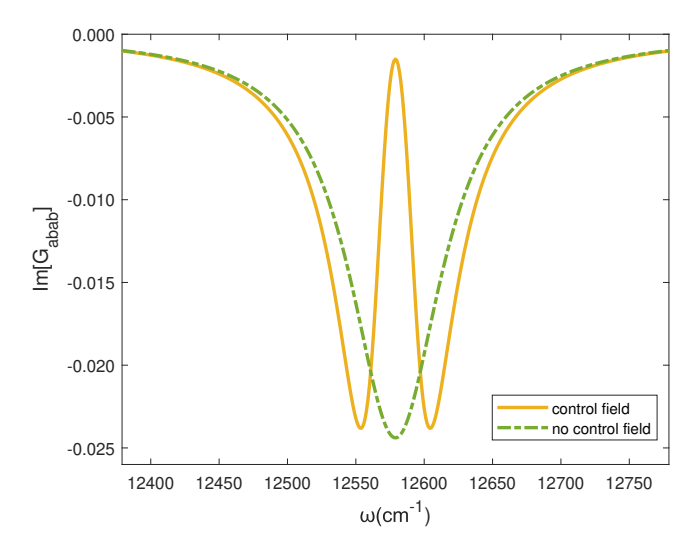


FIG. 3. Spectral plots of the imaginary part of $\mathcal{G}_{ab,ab}(\omega)$ in the presence or absence of the control field. The parameters are $\omega_{ab}=12579~\mathrm{cm}^{-1},~\Gamma_1=1~\mathrm{cm}^{-1},~\Gamma_2=0.0001~\mathrm{cm}^{-1},~\gamma_a^{(0)}=80~\mathrm{cm}^{-1},~\gamma_b^{(0)}=\gamma_c^{(0)}=1~\mathrm{cm}^{-1}$ and $\Omega=50~\mathrm{cm}^{-1}$.

where the Green's functions $\mathcal{G}_{ba,ba}(\omega_1)$ and $\mathcal{G}_{ab,ab}(\omega_3)$ have double peaks and a higher minimum with the presence of the control field than without, as shown in Fig. 3. By using the Green's functions, the rephasing and non-rephasing signals can be explicitly given as

$$S_{\text{rp}}^{(3)}(\omega_{3}, t_{2}, \omega_{1}) = \mathcal{G}_{ab,ab}(\omega_{3})\mathcal{G}_{aa,aa}(t_{2})\mathcal{G}_{ba,ba}(\omega_{1}) \\ + \mathcal{G}_{ab,ab}(\omega_{3})\mathcal{G}_{bb,aa}(t_{2})\mathcal{G}_{ba,ba}(\omega_{1}) \\ + \mathcal{G}_{ab,ab}(\omega_{3})\mathcal{G}_{aa,bb}(t_{2})\mathcal{G}_{ba,ba}(\omega_{1}) \\ + \mathcal{G}_{ab,ab}(\omega_{3})\mathcal{G}_{ba,bb}(t_{2})\mathcal{G}_{ba,ba}(\omega_{1}) (22) \\ S_{\text{nr}}^{(3)}(\omega_{3}, t_{2}, \omega_{1}) = \mathcal{G}_{ab,ab}(\omega_{3})\mathcal{G}_{aa,aa}(t_{2})\mathcal{G}_{ab,ab}(\omega_{1}) \\ + \mathcal{G}_{ab,ab}(\omega_{3})\mathcal{G}_{bb,aa}(t_{2})\mathcal{G}_{ab,ab}(\omega_{1}) \\ + \mathcal{G}_{ab,ab}(\omega_{3})\mathcal{G}_{aa,bb}(t_{2})\mathcal{G}_{ab,ab}(\omega_{1}) \\ + \mathcal{G}_{ab,ab}(\omega_{3})\mathcal{G}_{bb,bb}(t_{2})\mathcal{G}_{ab,ab}(\omega_{1}) (23)$$

We consider a case when the system is prepared at $|a\rangle$ after the first two pulses, cf. R_1 and R_2 in Fig. 2. After t_2 , the probability of the system remaining at $|a\rangle$ reads

$$\mathcal{G}_{aa,aa}(t_{2}) \simeq e^{-\frac{\gamma_{3}}{2}t_{2}} \left[\frac{1}{2} \cos\left(\widetilde{\Omega}t_{2}\right) \frac{A_{2}\Gamma_{2} + \Omega^{2}}{A_{1}} + \frac{1}{4} \sin\left(\widetilde{\Omega}t_{2}\right) \frac{A_{2}\Gamma_{2}\gamma_{3} + (\gamma_{3} - 2\Gamma_{1})\Omega^{2}}{i\widetilde{\Omega}A_{1}} \right] (24)$$

$$+ \frac{\Gamma_{2}}{2(\Gamma_{1} + \Gamma_{2})} + \frac{\Gamma_{1}(2A_{1} - \Omega^{2})e^{-(\Gamma_{1} + \Gamma_{2})t_{2}}}{2(\Gamma_{1} + \Gamma_{2})A_{1}},$$

$$\mathcal{G}_{bb,aa}(t_{2}) \simeq e^{-\frac{\gamma_{3}}{2}t_{2}} \left[\frac{1}{2} \cos\left(\widetilde{\Omega}t_{2}\right) \frac{A_{2}\Gamma_{1}}{A_{1}} + \frac{1}{4} \sin\left(\widetilde{\Omega}t_{2}\right) \frac{A_{2}\Gamma_{1}\gamma_{3} + 2\Omega^{2}}{i\widetilde{\Omega}A_{1}} \right]$$

$$+ \frac{\Gamma_{1}}{2(\Gamma_{1} + \Gamma_{2})} + \frac{\Gamma_{1}(\Omega^{2} - 2A_{1})e^{-(\Gamma_{1} + \Gamma_{2})t_{2}}}{2(\Gamma_{1} + \Gamma_{2})A_{1}},$$

where

$$A_1 = (\Gamma_1 + \Gamma_2)(\Gamma_1 + \Gamma_2 - \gamma_3) + \Omega^2,$$
 (26)

$$A_2 = \Gamma_1 + \Gamma_2 - \gamma_3, \tag{27}$$

$$\widetilde{\Omega} = \frac{1}{2} \sqrt{4\Omega^2 - \gamma_3^2}.$$
 (28)

When $\Omega = 0$, Eqs. (24) and (25) can be simplified as

$$\mathcal{G}_{aa,aa}(t_2) = \frac{\Gamma_2}{\Gamma_1 + \Gamma_2} + \frac{\Gamma_1}{\Gamma_1 + \Gamma_2} e^{-(\Gamma_1 + \Gamma_2)t_2}, (29)$$

$$G_{bb,aa}(t_2) = \frac{\Gamma_1}{\Gamma_1 + \Gamma_2} \left[1 - e^{-(\Gamma_1 + \Gamma_2)t_2} \right].$$
 (30)

In Fig. 4, we numerically plot $\mathcal{G}_{aa,aa}(t_2)$ and $\mathcal{G}_{bb,aa}(t_2)$ in the presence of the control field. It can be found that there is coherent population transfer between $|a\rangle$ and $|c\rangle$, after a time scale with $2/\gamma_3$, the coherent oscillations vanish, $\mathcal{G}_{aa,aa}(t_2)$ and $\mathcal{G}_{bb,aa}(t_2)$ finally approach a steady state $\Gamma_2/2(\Gamma_1 + \Gamma_2)$ and $\Gamma_1/2(\Gamma_1 + \Gamma_2)$. However, when the control field disappears, the coherent oscillation no longer exists, and the population in the $|a\rangle$ and $|b\rangle$ states monotonically change until they reach a steady state of $\Gamma_2/(\Gamma_1 + \Gamma_2)$ and $\Gamma_1/(\Gamma_1 + \Gamma_2)$.

Similarly, when the system is prepared at $|b\rangle$ after the first two pulses, cf. R_3 and R_4 in Fig. 2, the probability of the system remaining at $|b\rangle$ is

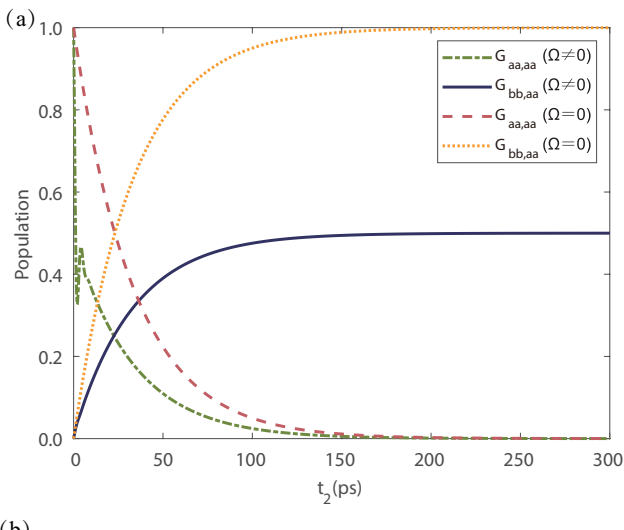
$$\mathcal{G}_{aa,bb}(t_2) \simeq \frac{\Gamma_2 - e^{-(\Gamma_1 + \Gamma_2)t_2} \Gamma_2}{\Gamma_1 + \Gamma_2},\tag{31}$$

$$\mathcal{G}_{bb,bb}(t_2) \simeq \frac{\Gamma_1 + e^{-(\Gamma_1 + \Gamma_2)t_2}\Gamma_2}{\Gamma_1 + \Gamma_2}.$$
 (32)

Since there is no control field applied to the transition between $|a\rangle$ and $|b\rangle$, there is no coherent oscillation of $\mathcal{G}_{aa,bb}(t_2)$ and $\mathcal{G}_{bb,bb}(t_2)$ as compared to $\mathcal{G}_{aa,aa}(t_2)$ and $\mathcal{G}_{bb,aa}(t_2)$. However, after a time scale with $1/(\Gamma_1 + \Gamma_2)$, they finally approach a steady state $\Gamma_2/(\Gamma_1 + \Gamma_2)$ and $\Gamma_1/(\Gamma_1 + \Gamma_2)$ as implied by the detailed balance.

III. RESULTS

We choose F=2 and F=3 for $5^2S_{1/2}$ of ^{85}Rb as the ground and metastable state and F=2 for $5^2P_{1/2}$ as the excited state. First of all, we shall plot the rephasing signal without the control field in Fig. 5. As shown, there is only one peak at $\omega_{ab}=\omega_a-\omega_b$. As the population time t_2 elapses, both the position and the height of the peak remains the same according to Eqs. (29), (30), (31), (32) and (22). This is because the number of atoms in the energy levels a and b is conserved. In other words, $\mathcal{G}_{aa,aa}(t_2) + \mathcal{G}_{bb,aa}(t_2) = 1$ and $\mathcal{G}_{aa,bb}(t_2) + \mathcal{G}_{bb,bb}(t_2) = 1$. When $t_2 \gg (\Gamma_1 + \Gamma_2)^{-1}$, the population transfer effectively ends. However, when the control field is applied, as shown in Fig. 6, the original one big peak is split into four small ones with widths significantly narrower than the original one due to the



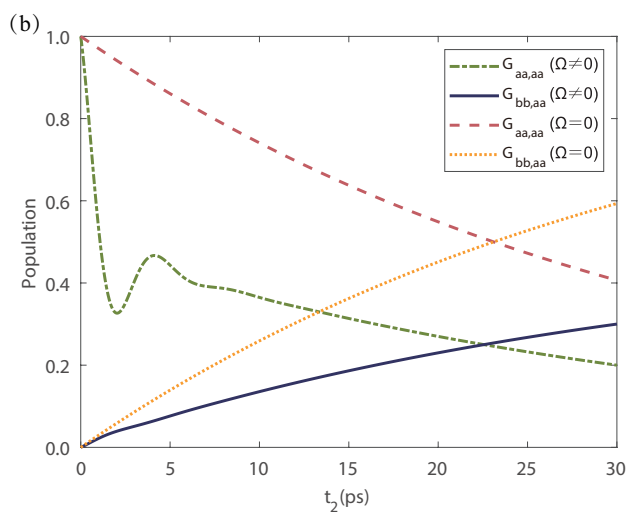


FIG. 4. In the presence and absence of a control field, population dynamics of $|a\rangle$ and $|b\rangle$. Sub-figure (b) is an enlarged view of (a) when t_2 is shortened. The other parameters are the same as in Fig. 3.

EIT effect. As shown in Fig. 3, the imaginary part of the Green functions in t_3 have been changed from single trough at $\omega_3 = \omega_{ab}$ to double troughs at

$$\omega_3 = \omega_{ab}$$

$$\pm \frac{1}{2} \sqrt{\frac{\Omega(\gamma_1 + \gamma_2)\sqrt{4\gamma_1\gamma_2 + \Omega^2} - \gamma_2(4\gamma_1\gamma_2 + \Omega^2)}{\gamma_1}} (33)$$

according to Eq. (21). The imaginary part of Green's function in t_1 will likewise change from one trough to two troughs. The reason for this phenomenon is given as follows. The larger the magnitude of the negative imaginary Green function is, the more the probe field is absorbed by the medium and thus the bigger the transition probability is. In the absence of the control field, the particle will only transit between the states $|b\rangle$ and $|a\rangle$. When the control field is applied, there are many different contributions to the transition paths, which start from $|b\rangle$ and end at $|a\rangle$, such as $|b\rangle \rightarrow |a\rangle \rightarrow |c\rangle \rightarrow |a\rangle$, $|b\rangle \rightarrow |a\rangle \rightarrow |c\rangle \rightarrow |a\rangle$ and so on. There will be interference between these transition

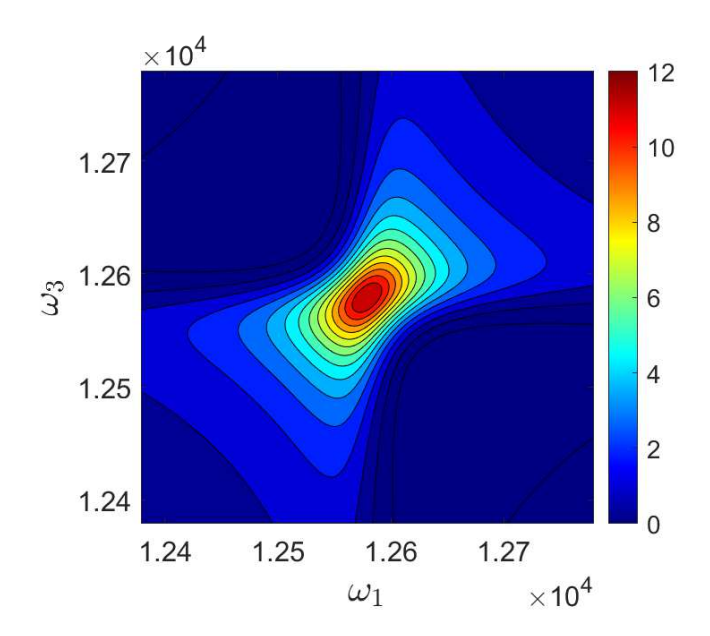


FIG. 5. In the absence of the control field, the 2D spectra of the rephasing signal. The parameters are the same as in Fig. 3.

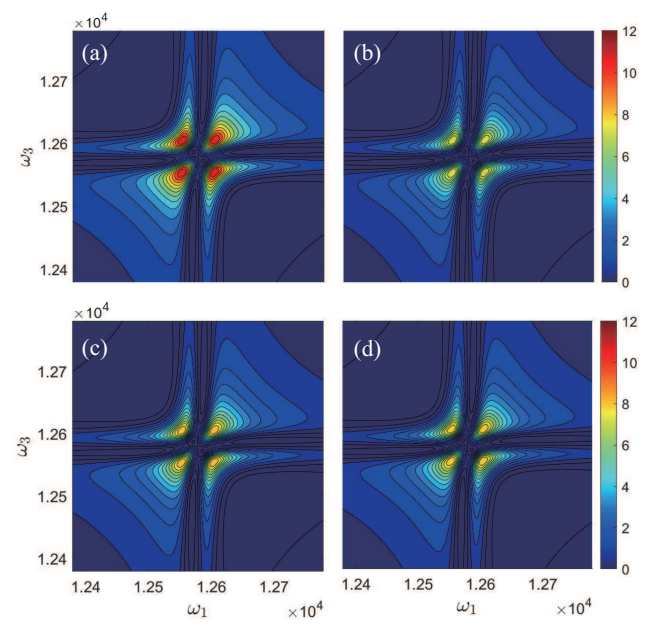


FIG. 6. In the presence of the control field, the 2D spectra of the rephasing signal for (a) $t_2 = 0$, (b) $t_2 = 2$ ps, (c) $t_2 = 4$ ps, and (d) $t_2 = 300$ ps. The parameters are the same as in Fig. 3.

paths, and the absorption of the probe field is the sum of the transition probability amplitudes of all paths. When the signs of the transition probability amplitudes are opposite to each other and thus cancel with each other, EIT is formed. Although both the shapes and the positions of these peaks will not be changed as t_2 is enlarged, the heights of the peaks decline and rise with $t_2 \sim 2/\gamma_3$ until steady state according to Eqs. (24), (25), (31), (32) and (22), which is similar to Fig. 4.

Then, we plot the non-rephasing signal in the absence

of the control field in Fig. 7. Because the states in the durations of t_1 and t_3 are the same for R_1 and R_4 , a trough appears at $\omega_1 = \omega_3 = \omega_{ab}$ in the two-dimensional spectroscopy in this case. The depth of the trough will not change with the extension of t_2 time, as can be seen from Eqs. (29), (30), (31), (32) and (23). When the control field is added, that is, EIT is introduced, one trough in the original two-dimensional spectroscopy will be split into four small troughs, as shown in Fig. 8. Equations (24), (25), (31), (32) and (23) imply that as t_2 time increases, the population in the a and b states will carry on the coherent oscillations with decreasing amplitude. After about 200 ps, the populations of both a and b states become stable. Hence, both the position and shape of the troughs do not change in the spectroscopy, but their depths oscillate with the passage of t_2 time.

Summing the rephasing and non-rephasing signals, the total absorptive 2D spectroscopy is obtained, which is more complicated as can be seen from Fig. 9. There are two peaks along the diagonal line, and two troughs along the anti-diagonal line. Moreover, with the increase of t_2 time, the atoms in the a and b energy levels transition to each other, but the overall height of the peaks and the depth of the troughs remain the same. When the control field is added, as shown in Fig. 10, in addition to the above two sets of main peaks and troughs, two new sets of peaks and troughs emerge, i.e., eight narrow peaks and troughs between one main peak and trough, and four small ones at the center. Similar to the rephasing and non-rephasing signals, the time evolution of both the peaks and troughs shows damped oscillation and they finally arrive at the steady state in the long-time limit. Neither the number nor the positions of the peaks and troughs in the 2DES change due to the elapse of t_2 . It implies that both the rephasing and non-rephasing spectroscopy possess the shape over ω_1 and ω_3 , although the magnitude changes over time.

IV. CONCLUSION

In this paper, we apply EIT which can induce constructive and destructive interference to two-dimensional spectroscopy. It is found that in the rephasing and nonrephasing signals, the original one large peak (trough) is split into four small peaks (troughs). With the evolution of the population time, the height of the peaks (the depth of the troughs) will rise and fall until a steady value in the long-time limit due to the transition of the atoms. But both the position and shape of the peak (trough) will not change during the evolution. The time evolution of the absorptive signal will show a similar characteristic although its spectroscopy is much more complicated. This means that EIT can improve the resolution of 2DES, and this method is promising to obtain more information about excited state dynamics.

Acknowledgments.— This work is supported by Beijing Natural Science Foundation under Grant No. 1202017

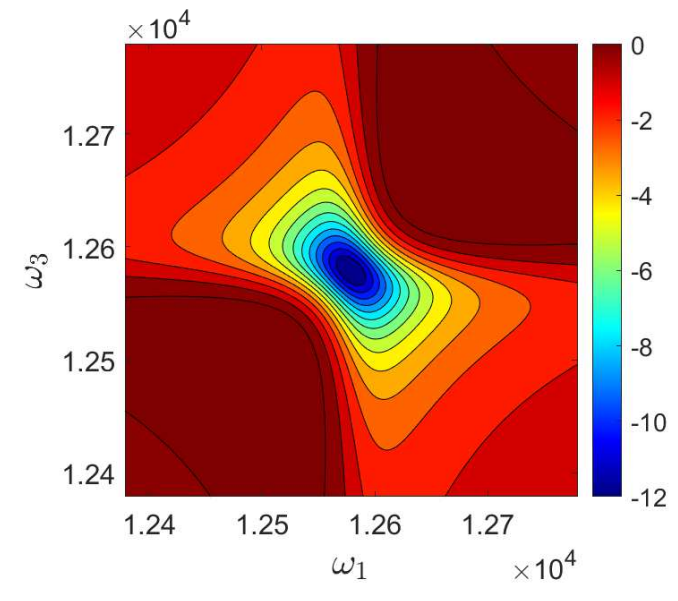


FIG. 7. In the absence of the control field, the 2D spectra of the non-rephasing signal. The other parameters are the same as in Fig. 3.

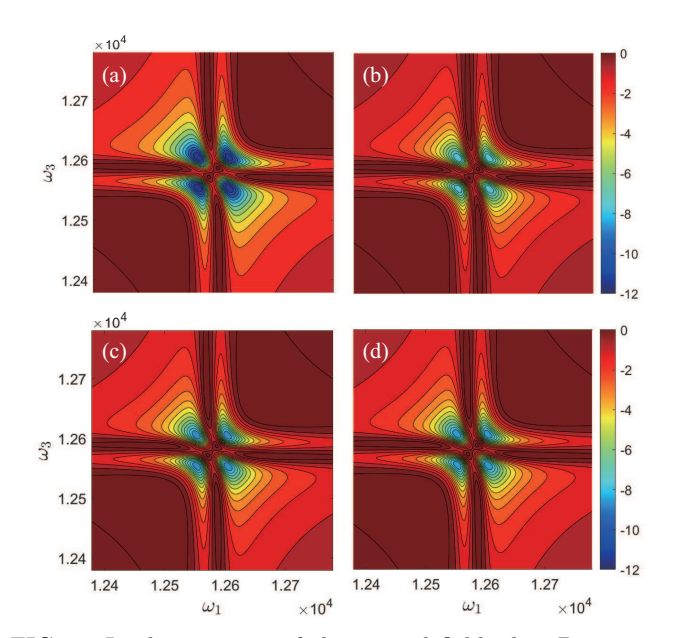


FIG. 8. In the presence of the control field, the 2D spectra of the non-rephasing signal for (a) $t_2 = 0$, (b) $t_2 = 2$ ps, (c) $t_2 = 4$ ps, and (d) $t_2 = 300$ ps. The other parameters are the same as in Fig. 3.

and the National Natural Science Foundation of China under Grant Nos. 11674033, 11505007, and Beijing Normal University under Grant No. 2022129.

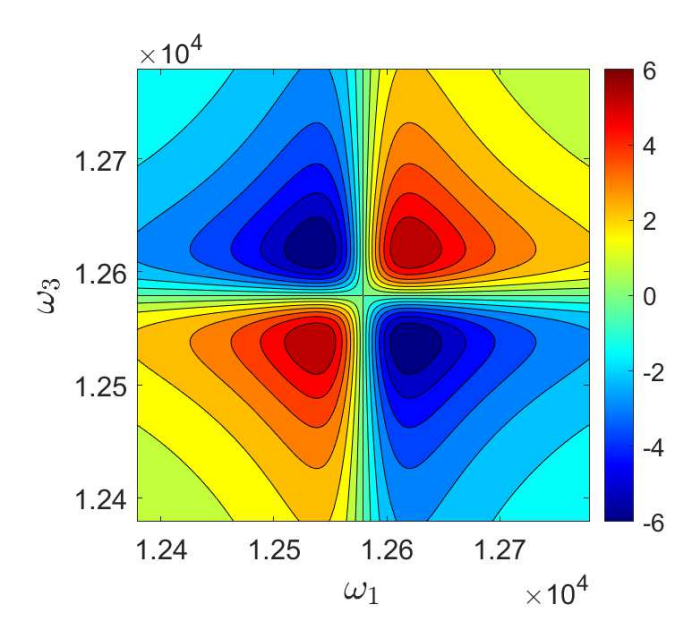


FIG. 9. In the absence of the control field, the 2D spectra of the absorptive signal. The other parameters are the same as in Fig. 3.

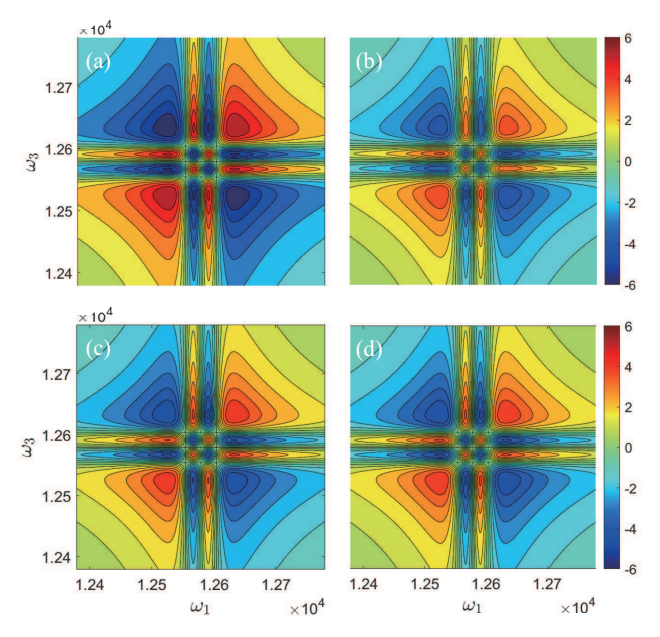


FIG. 10. In the presence of the control field, the 2D spectra of the absorptive signal for (a) $t_2 = 0$, (b) $t_2 = 2$ ps, (c) $t_2 = 4$ ps, and (d) $t_2 = 300$ ps. The other parameters are the same as in Fig. 3.

^[1] M. O. Scully and M. S. Zubairy, *Quantum Optics* (Cambridge University Press, New York, 1997).

^[2] S. A. Hopkins, E. Usadi, H. X. Chen, and A. V. Durrant, "Electromagnetically induced transparency of lasercooled rubidium atoms in three-level Λ-type systems," Opt. Commun. 138, 185 (1997).

^[3] L. V. Hau, S. E. Harris, Z. Dutton, and C. H. Behroozi, "Light speed reduction to 17 metres per second in an ultracold atomic gas," Nature 397, 594 (1999).

^[4] B.-W. Shiau, M.-C. Wu, C.-C. Lin, and Y.-C. Chen, "Low-light-level cross-phase modulation with double slow light pulses," Phys. Rev. Lett. 106, 193006 (2011).

- [5] H. Schmidt and A. Imamoğlu, "Nonlinear optical devices based on a transparency in semiconductor intersubband transitions," Opt. Commun. 131, 333 (1996).
- [6] Y. Zhao, C.-K. Wu, B.-S. Ham, M. K. Kim, and E. Awad, "Microwave induced transparency in ruby," Phys. Rev. Lett. 79, 641 (1997).
- [7] E. Kuznetsova, O. Kocharovskaya, P. Hemmer, and M. O. Scully, "Atomic interference phenomena in solids with a long-lived spin coherence," Phys. Rev. A 66, 063802 (2002).
- [8] E. Baldit, K. Bencheikh, P. Monnier, S. Briaudeau, J. A. Levenson, V. Crozatier, I. Lorgeré, F. Bretenaker, J. L. Le Gouët, O. Guillot-Noël, and Ph. Goldner, "Identification of Λ-like systems in Er³⁺: Y₂SiO₅ and observation of electromagnetically induced transparency," Phys. Rev. B 81, 144303 (2010).
- [9] H.-Q. Fan, K. H. Kagalwala, S. V. Polyakov, A. L. Migdall, and E. A. Goldschmidt, "Electromagnetically induced transparency in inhomogeneously broadened solid media," Phys. Rev. A 99, 053821 (2019).
- [10] C.-J. Wei and N. B. Manson, "Observation of the dynamic stark effect on electromagnetically induced transparency," Phys. Rev. A 60, 2540 (1999).
- [11] P. R. Hemmer, A. V. Turukhin, M. S. Shahriar, and J. A. Musser, "Raman-excited spin coherences in nitrogenvacancy color centers in diamond," Opt. Lett. 26, 361 (2001).
- [12] V. M. Acosta, K. Jensen, C. Santori, D. Budker, and R. G. Beausoleil, "Electromagnetically induced transparency in a diamond spin ensemble enables alloptical electromagnetic field sensing," Phys. Rev. Lett. 110, 213605 (2013).
- [13] Y.-Y. Wang, J. Qiu, Y.-Q. Chu, M. Zhang, J.-M. Cai, Q. Ai, and F.-G. Deng, "Dark state polarizing a nuclear spin in the vicinity of a nitrogen-vacancy center," Phys. Rev. A 97, 042313 (2018).
- [14] M. Fleischhauer and M. D. Lukin, "Dark-state polaritons in electromagnetically induced transparency," Phys. Rev. Lett. 84, 5094 (2000).
- [15] C. Liu, Z. Dutton, C. H. Behroozi, and L. V. Hau, "Observation of coherent optical information storage in an atomic medium using halted light pulses," Nature 409, 490 (2001).
- [16] M. Fleischhauer and M. D. Lukin, "Quantum memory for photons: Dark-state polaritons," Phys. Rev. A 65, 022314 (2002).
- [17] K. Honda, D. Akamatsu, M. Arikawa, Y. Yokoi, K. Akiba, S. Nagatsuka, T. Tanimura, A. Furusawa, and M. Kozuma, "Storage and retrieval of a squeezed vacuum," Phys. Rev. Lett. 100, 093601 (2008).
- [18] Y.-F. Hsiao, P.-J. Tsai, H.-S. Chen, S.-X. Lin, C.-C. Hung, C.-H. Lee, Y.-H. Chen, Y.-F. Chen, A. Y. Ite, and Y.-C. Chen, "Highly efficient coherent optical memory based on electromagnetically induced transparency," Phys. Rev. Lett. 120, 183602 (2018).
- [19] Y.-H. Chen, M.-J. Lee, I.-C. Wang, S.-W. Du, Y.-F. Chen, Y.-C. Chen, and A. Y. Ite, "Coherent optical memory with high storage efficiency and large fractional delay," Phys. Rev. Lett. 110, 083601 (2013).
- [20] N. Kukharchyk, D. Sholokhov, O. Morozov, S. L. Korableva, A. A. Kalachev, and P. A. Bushev, "Electromagnetically induced transparency in a mono-isotopic ¹⁶⁷Er: ⁷LiYF₄ crystal below 1 Kelvin: microwave photonics approach," Opt. Express 28, 29166 (2020).

- [21] J. Wang, W.-T. He, C.-W. Lu, Y.-Y. Wang, Q. Ai, and H.-B. Wang, "Controlled-not gate based on the rydberg states of surface electrons," Ann. Phys. (Berlin) 535, 2300138 (2023).
- [22] X.-R. Jin, Y.-Q. Zhang, S. Zhang, Y.-P. Lee, and J.-Y. Rhee, "Polarization-independent electromagnetically induced transparency-like effects in stacked metamaterials based on Fabry-Perot resonance," J. Optics 15, 125104 (2013).
- [23] F. Bagci and B. Akaoglu, "Transmission control by asymmetric electromagnetically induced transparencylike metamaterials in transverse electromagnetic waveguide," Phys. Lett. A 383, 126000 (2019).
- [24] X.-R. Jin, Y.-H. Lu, H.-Y. Zheng, Y.-P. Lee, J.-Y. Rhee, K.-W. Kim, and W.-H. Jang, "Plasmonic electromagnetically-induced transparency in metamaterial based on second-order plasmonic resonance," Opt. Commun. 284, 4766 (2011).
- [25] P. Tassin, L. Zhang, Th. Koschny, E. N. Economou, and C. M. Soukoulis, "Low-loss metamaterials based on classical electromagnetically induced transparency," Phys. Rev. Lett. 102, 053901 (2009).
- [26] H. Xu, Y.-H. Lu, Y.-P. Lee, and B.-S. Ham, "Studies of electromagnetically induced transparency in metamaterials," Opt. Express 18, 17736 (2010).
- [27] H.-B. Huang, J.-J. Lin, Y.-X. Yao, K.-Y. Xia, Z.-Q. Yin, and Q. Ai, "Optical nonreciprocity in rotating diamond with nitrogen-vacancy color centers," Ann. Phys. (Berlin) 534, 2200157 (2022).
- [28] K.-J. Boller, A. Imamoğlu, and S. E. Harris, "Observation of electromagnetically induced transparency," Phys. Rev. Lett. 66, 2593 (1991).
- [29] S. Mukamel, Principles of Nonlinear Optics and Spectroscopy (Oxford University Press, New York, 1999).
- [30] G. S. Schlau-Cohen, A. Ishizaki, and G. R. Fleming, "Two-dimensional electronic spectroscopy and photosynthesis: Fundamentals and applications to photosynthetic light-harvesting," Chem. Phys. 386, 1 (2011).
- [31] F. D. Fuller and J. P. Ogilvie, "Experimental implementations of two-dimensional fourier transform electronic spectroscopy," Annu. Rev. Phys. Chem. 66, 667 (2015).
- [32] Z.-H. Sun, Y.-X. Yao, Q. Ai, and Y.-C. Cheng, "Theory of center-line slope in 2D electronic spectroscopy with static disorder," Adv. Quantum Technol. 6, 2300163 (2023).
- [33] G.-Y. Liu, A. S. Sizhuk, and K. E. Dorfman, "Selective elimination of homogeneous broadening by multidimensional spectroscopy in the electromagnetically induced transparency regime," J. Phys. Chem. Lett. 11, 5504 (2020).
- [34] H. Seiler, S. Palato, C. Sonnichsen, H. Baker, and P. Kambhampati, "Seeing multiexcitons through sample inhomogeneity: Band-edge biexciton structure in cdse nanocrystals revealed by two-dimensional electronic spectroscopy," Nano Lett. 18, 2999. (2018).
- [35] P. Brosseau, S. Palato, H. Seiler, H. Baker, and P. Kambhampati, "Fifth-order two-quantum absorptive two-dimensional electronic spectroscopy of CdSe quantum dots," J. Chem Phys. 153, 234703 (2020).
- [36] G. Moody, C. Kavir Dass, K. Hao, C.-H. Chen, L.-J. Li, A. Singh, K. Tran, G. Clark, X.-D. Xu, G. Berghäuser, E. Malic, A. Knorr, and X.-Q. Li, "Intrinsic homogeneous linewidth and broadening mechanisms of excitons in monolayer transition metal

- dichalcogenides," Nat. Commun. 6, 8315 (2015).
- [37] L. Guo, M. Wu, T. Cao, D. M. Monahan, Y.-H. Lee, S. G. Louie, and G. R. Fleming, "Exchange-driven intravalley mixing of excitons in monolayer transition metal dichalcogenides," Nat. Phys. 15, 228 (2019).
- [38] A. Jha, H.-G. Duan, V. Tiwari, P. K. Nayak, H. J. Snaith, M. Thorwart, and R. J. D. Miller, "Direct observation of ultrafast exciton dissociation in lead iodide perovskite by 2D electronic spectroscopy," Acs Photonics 5, 852 (2017).
- [39] D. M. Monahan, L. Guo, J. Lin, L.-T. Dou, P.-D. Yang, and G. R. Fleming, "Room-temperature coherent optical phonon in 2D electronic spectra of CH₃NH₃PbI₃ perovskite as a possible cooling bottleneck," J. Phys. Chem. Lett. 8, 3211 (2017).
- [40] H. Seiler, S. Palato, C. Sonnichsen, H. Baker, E. Socie, D. P. Strandell, and P. Kambhampati, "Twodimensional electronic spectroscopy reveals liquid-like lineshape dynamics in cspbi3 perovskite nanocrystals," Nat. Commun. 10, 4962 (2019).
- [41] T. R. Calhoun, N. S. Ginsberg, G. S. Schlau-Cohen, Y.-C. Cheng, M. Ballottari, R. Bassi, and G. R. Fleming, "Quantum coherence enabled determination of the energy landscape in light-harvesting complex II," J. Phys. Chem. B 113, 16291 (2009).
- [42] F. D. Fuller, J. Pan, A. Gelzinis, V. Butkus, S. S. Senlik, D. E. Wilcox, C. F. Yocum, L. Valkunas,

- D. Abramavicius, and J. P. Ogilvie, "Vibronic coherence in oxygenic photosynthesis," Nat. Chem. 6, 706 (2014).
- [43] S.-H. Jun, C.-H. Yang, M. Isaji, H. Tamiaki, J.-H. Kim, and H. Ihee, "Coherent oscillations in chlorosome elucidated by two-dimensional electronic spectroscopy," J. Phys. Chem. Lett. 5, 1386 (2014).
- [44] E. Romero, R. Augulis, V. I. Novoderezhkin, M. Ferretti, J. Thieme, D. Zigmantas, and R. van Grondelle, "Quantum coherence in photosynthesis for efficient solarenergy conversion," Nat. Phys. 10, 676 (2014).
- [45] S.-H. Jun, C.-H. Yang, T.-W. Kim, M. Isaji, H. Tamiaki, H. Ihee, and J.-H. Kim, "Role of thermal excitation in ultrafast energy transfer in chlorosomes revealed by two-dimensional electronic spectroscopy," Phys. Chem. Chem. Phys. 17, 17872 (2015).
- [46] F. Ma, L.-J. Yu, R. Hendrikx, Z. Y. Wang Otomo, and R. van Grondelle, "Excitonic and vibrational coherence in the excitation relaxation process of two LH1 complexes as revealed by two-dimensional electronic spectroscopy," J. Phys. Chem. Lett. 8, 2751 (2017).
- [47] E. Thyrhaug, R. Tempelaar, M. J. P. Alcocer, K. Žídek, D. Bína, J. Knoester, T. L. C. Jansen, and D. Zigmantas, "Identification and characterization of diverse coherences in the Fenna–Matthews–Olson complex," Nat. Chem. 10, 780 (2018).
- [48] H. P. Breuer and F. Petruccione, The Theory of Open Quantum Systems (Oxford University Presss, 2002).